Available online at www.sciencedirect.com
ScienceDirect
International Journal of Heat and Mass Transfer 51 (2008) 2772–2783
International Journal of HEAT and MASS TRANSFER
www.elsevier.com/locate/ijhmt

Inverse radiation analysis using repulsive particle swarm optimization algorithm

Kyun Ho Lee [a,*], Seung Wook Baek [a], Ki Wan Kim [b]

[a] Department of Aerospace Engineering, School of Mechanical, Aerospace and Systems Engineering, Korea Advanced Institute of Science and Technology, 373-1 Guseong-dong, Yuseong-gu, Daejeon 305-701, Republic of Korea
[b] Agency for Defense Development, 462 Jochiwongil, Yuseong-gu, Daejeon 305-600, Republic of Korea

Received 29 June 2007; received in revised form 15 September 2007
Available online 4 December 2007

Abstract

In this study, an inverse radiation analysis is presented for the estimation of the radiation properties for an absorbing, emitting, and scattering media with diffusely emitting and reflecting opaque boundaries. The repulsive particle swarm optimization (RPSO) algorithm, which is a relatively recent heuristic search method, is proposed as an effective method for improving the search efficiency for unknown radiative parameters. To verify the performance of the RPSO algorithm, it is compared with a basic particle swarm optimization (PSO) algorithm and a hybrid genetic algorithm (HGA) for the inverse radiation problem in estimating the various radiation properties in a two-dimensional irregular medium, when the temperatures are given at only four measurement positions. A finite-volume method is applied to solve the radiative transfer equation of a direct problem to obtain measured temperatures. RPSO is proven to be quite a robust tool for simultaneous estimation of multi-parameters even in a strongly-coupled environment.

Keywords: Inverse radiation analysis; Repulsive particle swarm optimization; Hybrid genetic algorithm; Parameter estimation; Irregular geometry; Finite-volume method

1. Introduction

In recent years, the inverse heat transfer analyses provide a great advantage where desired quantities are not possible to be measured directly from experiments, for example, high surface temperatures on a reentry vehicle or thermal properties of hot gas during combustion, etc. [1]. Especially for inverse radiation analyses, many studies have been concerned with the determination of the radiation properties, boundary condition and temperature profile or source term distribution, given various types of radiation measurements [2–4]. Unfortunately the solution obtained from inverse analyses may neither exist, nor be unique. Using given measurement data with some error, the inverse problems cannot be directly solved. Therefore, various mathematical methods have been adopted to obtain a stable solution in spite of the ill-posed characteristic of inverse problem. Among them, the conjugate gradient method (CGM) has usually been adopted by many researchers in inverse heat problems [5–7]. The CGM has an advantage of stably estimating the solutions in relatively short computational time, but complex mathematical equations such as sensitivity and adjoint problems should be additionally solved together. Also, the unfeasible solutions can be obtained if initial values are not guessed properly or if the parameters are highly correlated, the iteration number for the parameter estimation increases until they converge [8]. As an alternative to gradient-based methods, search-based methods, such as genetic algorithm (GA) and particle swarm optimization (PSO) have received much

* Corresponding author. Tel.: +82 42 860 2936; fax: +82 42 860 2603.
E-mail address: khlee0406@kaist.ac.kr (K.H. Lee).

0017-9310/$ - see front matter © 2007 Elsevier Ltd. All rights reserved.
doi:10.1016/j.ijheatmasstransfer.2007.09.037

Nomenclature

a_I^m	coefficient of discretization equation
b_P^m	source in discretization equation
c_i	acceleration coefficient
D_{ci}^m	directional weights
E_b	blackbody emissive power, W/m^2
I	radiation intensity, W/(m^2 sr)
M	number of total radiation direction
$\vec{n}_i$	unit normal vector at surface i
$P_j(\,)$	Legendre polynomial of order j
p_i^k	local best position of ith particle at k
p_g^k	global best position of swarm at k
q^R	radiative heat flux, W/m^2
r_i	uniform random number $[0,1]$
S_{nr}	volumetric heat source, W/m^3
S_R^{mn}	source term in FVM
s	distance traveled by a ray, m
$\vec{s}$	unit direction vector
T	temperature, K
v_i^k	velocity of ith particle at iteration k
v_r	random velocity
w	inertia weight
x_i^k	position of ith particle at iteration k

Greek symbols

β_0	extinction coefficient, m^{-1}
ΔA_i	surface area of the ith control surface
ΔV	volume of the control volume
$\Delta\Omega$	control angle, sr
ε_w	wall emissivity
θ	polar angle, rad
κ_a	absorption coefficient, m^{-1}
μ,η	direction cosines
σ	Stefan–Boltzmann constant, 5.67×10^{-8} W/(m^2 K^4)
σ_s	scattering coefficient, m^{-1}
$\mathbf{\Phi}$	scattering phase function, sr^{-1}
ϕ	azimuthal angle
$\mathbf{\Psi}$	scattering angle between $\vec{s}'$, $\vec{s}$
Ω	solid angle, sr
ω_0	single scattering albedo

Superscripts

k	number of iteration
mn	radiation direction

Subscripts

i	ith particle
P	calculating nodal point

attention for outstanding characteristics, especially in non-linear or multi-parameter problems. Li and Yang used GA in inverse radiation analysis for estimating the scattering albedo, optical thickness and phase function in parallel plane [9], while Kim et al. estimated wall emissivities with hybrid genetic algorithm [10]. Becceneri et al. implemented PSO for estimating radiative properties in a 1D plane-parallel participating medium [11]. Although these methods have been successfully applied to various inverse problems with high computing resources recently, it still takes a longer computing time than gradient-based methods.

In this study, to solve efficiently the inverse problems which are highly non-linear, non-monotonic, or a very complex form, the repulsive particle swarm optimization (RPSO) is adopted as a fast, robust and stable inverse method rather than the other search-based ones. To verify the feasibility and the performance of RPSO, it is applied to inverse radiation analysis in estimating the wall emissivities, absorption and scattering coefficients in a 2D absorbing, emitting and scattering irregular medium with measured temperatures. Also, the accuracy of estimated parameters and the computational efficiency are compared with the results obtained from HGA and PSO techniques.

2. Principle of algorithm

2.1. Hybrid genetic algorithm (HGA)

Genetic algorithm (GA) is a well known global optimization technique based on the Darwin's principle of the 'survival of the fittest' and the natural process of evolution [12]. Generally, it starts with a randomly generated population of candidate solutions (individuals) within some ranges and then exchanges genetic information between individuals to reproduce improved solutions from one generation to the next by three simulated evolution processes, which are selection, crossover and mutation. By repeating them, the better individuals are reproduced while the bad ones are extinguished at each generation. If a desirable fitness of an object function is obtained, then the best individuals of the last generation are regarded as the final solution. Based on its ability to reach global optima, the GA has been extensively applied in many engineering fields such as optimization and fuzzy logic control [13,14].

However, the GA has some drawbacks such as inability to perform fine local tuning due to its poor exploitation, a premature convergence to a non-global optimum and a longer computing time. Also, a proper selection of population size, crossover and mutation probabilities, and the

maximum number of generations is required because they greatly affect the performance of GA. To overcome these difficulties, an elitist strategy and a local optimization algorithm (LOA) are combined with a simple GA, which is thereby so-called hybrid genetic algorithm (HGA). The elitist strategy ensures monotonic improvement in the best fitness value of each generation and helps to reach near the global optima while LOA helps faster converge to them. The LOA is applied to only elite individual to reduce computation time after determining the elite individual. If $s = \langle v_1, v_2, \ldots, v_m \rangle$ is a chromosome of elite individual and the gene v_k is selected for local optimization, the resulting gene v'_k is as follows:

$$v'_k = \begin{cases} v_k + \Delta(t, UB - v_k) \\ v_k - \Delta(t, v_k - LB) \end{cases} \quad (1)$$

The function $\Delta(t,y)$ returns a value in the range $[0,y]$ such that the probability of $\Delta(t,y)$, being close to 0, increases as t increases. The following function is used for $\Delta(t,y)$

$$\Delta(t,y) = y \cdot \left(1 - r^{\left(1-\frac{t}{T_{\max}}\right)^b}\right) \quad (2)$$

where r is a uniform random number, $T_{\max}$ is the maximum generation number, and b is a system parameter for determining the degree of dependency on generation number, t ($b = 1$ here). In LOA, using Eq. (1) v'_k is calculated for each gene of elite individual. If v'_k is fitter than v_k, gene of elite individual is changed to v'_k. Otherwise, v_k is maintained. A more detailed description of HGA can be found in Ref. [10], and its flowchart is presented in Fig. 1(a).

2.2. Particle swarm optimization (PSO)

Particle swarm optimization (PSO) is a recent high performance algorithm created as an alternative to the GA. It is based on the social behavior of a swarm of birds or a school of fish which searches for food in a very typical manner. If an individual of the swarm sees a desirable path to go, the rest will follow quickly. Every member of the swarm searches for the best in its locality-learns from its own experience. Additionally, each member learns from the others, typically from the best performer among them [15]. The PSO consists of three steps, namely, generating positions and velocities of particles, velocity update, and finally, position update. The flowchart of PSO is presented in Fig. 1(b) and its detailed procedures are as follows:

(1) Randomly initialize the velocities and the positions of all particles within expected ranges.
(2) At current kth iteration, the velocity of ith particle for next iteration is updated according to following equation:

$$v_i^{k+1} = w v_i^k + c_1 r_1 (p_i^k - x_i^k) + c_2 r_2 (p_g^k - x_i^k) \quad (3)$$

where x_i^k and v_i^k are the position and velocity of particle i. p_i^k and p_g^k are the positions with the best objective value found so far by particle i and by all particles, which are called the local and the global best position, respectively. w is an inertia factor which controls the flying dynamics, r_i, r_2 are uniform random variables in the range $[0,1]$. Also c_1, c_2 are acceleration coefficients that pull each particle toward the local and the global best positions. From Eq. (3), the current and the best information of particle and swarm are considered all together to update velocities of all particles for next iteration, which are totally different from GA.

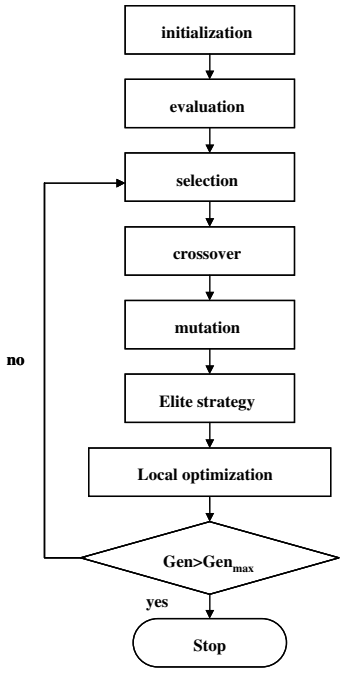

(a) Hybrid genetic algorithm

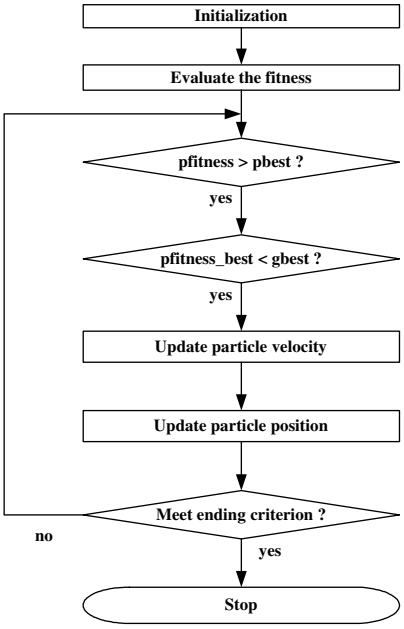

(b) Particle swarm optimization algorithm

Fig. 1. The flowchart of search-based algorithm.

(3) Finally, after updating the position of each particle using its new velocity for unit time by

$$x_i^{k+1} = x_i^k + v_i^{k+1} \tag{4}$$

(4) Repeat the velocity update, position update, and fitness calculations until meeting a desired convergence criterion (a sufficiently good fitness or a maximum number of iterations).

Similar to GA, the PSO is firstly initialized in a set of randomly generated potential solutions (particles), and then iteratively performs the search for the optimum one. But unlike GA, every particle flies through the search space with velocity which is dynamically adjusted according to its own and companions' flying. Namely, the particles have a tendency to fly towards the better and better search area without using the complex techniques of GA. Compared to GA, the PSO is much simpler, can be easily implemented, has fewer parameters to adjust and is computationally inexpensive since its memory and CPU speed requirements are low [16]. Furthermore, it does not require gradient information of the objective function. Based on these advantages, the PSO has been successfully applied to solve a lot of practical applications such as function optimization, artificial neural network training, pattern recognition, fuzzy control and some other fields in recent years [17].

2.3. Repulsive particle swarm optimization (RPSO)

Despite the above advantages, the PSO can stop evolution and rather fall into premature convergence especially for complex problems with many local optima and optimization parameters [18]. Therefore, various variant models of PSO have been developed recently to improve its performance, and to increase the diversity of particles of the original PSO [19]. Among such variants, the repulsive particle swarm optimization (RPSO) method, which is developed to implement the repulsion between particles, is particularly effective in finding out the global optimum in very complex search spaces. The main difference between PSO and RPSO is the propagation mechanism to determine new velocity for a particle as follows:

$$v_i^{k+1} = wv_i^k + c_1 r_1 (p_i^k - x_i^k) + c_2 r_2 w(p_j^k - x_i^k) + c_3 r_3 w v_r \tag{5}$$

where p_i^k is the local best position of particle i, and p_j^k is the local best position of a randomly chosen other particle among the swarm. Also, c_1, c_2, c_3 are acceleration coefficients and v_r indicates a random velocity component. The second term on the right side of Eq. (5) leads to a motion of the particle towards its best position while the third term leads to a repulsion between the particle and the best position of a randomly chosen other particle in order to explore new areas and to prevent the population to get stuck in a local optimum. The fourth term generates noise in the velocity of a particle to enhance the exploration to new areas in the search space. Consequently, the RPSO can prevent the swarm from being trapped in local minimum, which would cause a premature convergence and lead to fail in finding the global optimum. Instead, it is capable of finding global optima in more complex search spaces [20].

3. Mathematical formulation

3.1. Physical model

Fig. 2 shows an irregular quadrilateral enclosure which is filled with an absorbing, emitting, scattering and gray gas with κ_a and σ_s [10]. The non-radiative volumetric heat source is $\dot{Q} = 5.0\ \mathrm{kW/m^3}$. The walls are gray and their temperatures are all $T_w = 1000\ \mathrm{K}$. The spatial and angular domains are discretized into $(N_x \times N_y) = 10 \times 10$ control volumes and $(N_\theta \times N_\phi) = 4 \times 20$ control angles corresponding to S_8 quadrature scheme [21]. The temperature distribution in gray gas is determined from the following energy equation [22]:

$$\nabla \cdot q_r = \beta_0 (1 - \omega_0) \left(4\pi I_b - \sum_{n=1}^{N_\phi} \sum_{m=1}^{N_\theta} I^{mn} \Delta\Omega^{mn} \right) = \dot{Q} \tag{6}$$

3.2. Direct problem

The radiative transfer equation governing radiation intensity for a gray medium at any position $\mathbf{r}$ along a path $\mathbf{s}$ through an absorbing, emitting, and scattering medium is given by

$$\frac{1}{\beta_0} \frac{\mathrm{d}I(\mathbf{r},\mathbf{s})}{\mathrm{d}s} + I(\mathbf{r},\mathbf{s}) = (1-\omega_0) I_b(\mathbf{r}) + \frac{\omega_0}{4\pi} \times \int_{\Omega'=4\pi} I(\mathbf{r},\mathbf{s}') \Phi(\mathbf{s}' \to \mathbf{s}) \mathrm{d}\Omega' \tag{7}$$

where $\beta_0 = \kappa_a + \sigma_s$ is the extinction coefficient, and $\omega_0 = \sigma_s/\beta_0$ is the scattering albedo. $\Phi(\mathbf{s}' \to \mathbf{s})$ is the scattering phase function for radiation from incoming direction $\mathbf{s}'$

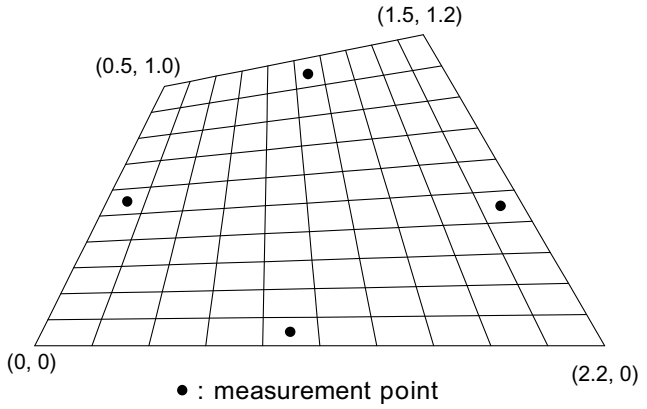

Fig. 2. Schematic of the physical system and the position of four measurement points.

to scattered direction **s**. It is approximated by a finite series of Legendre polynomial as

$$\mathbf{\Phi}(\mathbf{s}' \to \mathbf{s}) = \mathbf{\Phi}(\cos\mathbf{\Psi}) = \sum_{j=0}^{J} C_j P_j(\cos\mathbf{\Psi}) \tag{8}$$

where C_j is the expansion coefficient, and J is the order of the phase function. The boundary condition for a diffusely emitting and reflecting wall can be written as follows:

$$I(\mathbf{r}_\mathrm{w}, \mathbf{s}) = \varepsilon_\mathrm{w} I_\mathrm{b}(\mathbf{r}_\mathrm{w}) + \frac{1-\varepsilon_\mathrm{w}}{\pi} \int_{\mathbf{s}'\cdot\mathbf{n}_\mathrm{w}<0} I(\mathbf{r}_\mathrm{w}, \mathbf{s}')|\mathbf{s}'\cdot\mathbf{n}_\mathrm{w}|\mathrm{d}\Omega' \tag{9}$$

where ε_w is the wall emissivity and $\mathbf{n}_\mathrm{w}$ is the unit normal vector to the wall.

To derive the finite-volume discretization equation, Eq. (7) is integrated over a control volume, ΔV and a control angle, $\Delta\Omega^{mn}$, as shown in Fig. 3. By assuming that the magnitude of the intensity is constant but its direction varies within the control volume and control angle given, the following finite-volume formulation can be obtained:

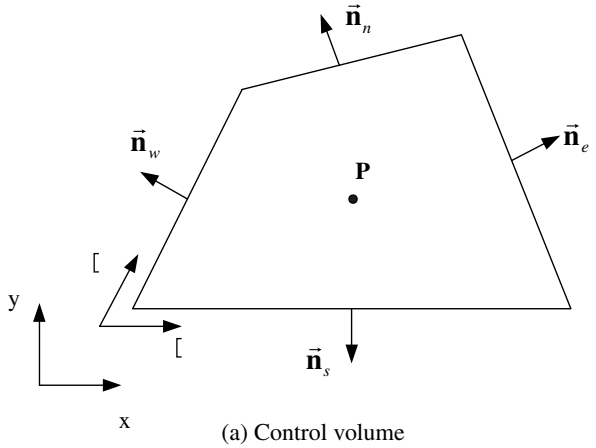

(a) Control volume

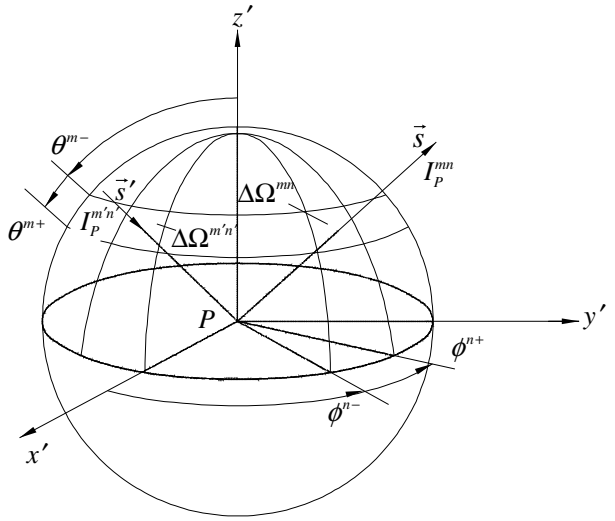

(b) Control angle

Fig. 3. Schematics of finite-volume grids.

$$\sum_{i=e,w,n,s} I_i^{mn} \Delta A_i D_{ci}^{mn} = \beta_0(-I^{mn} + S_\mathrm{R}^{mn})_P \Delta V \Delta\Omega^m \tag{10a}$$

where

$$D_{ci}^{mn} = \int_{\phi^{n-}}^{\phi^{n+}} \int_{\theta^{m-}}^{\theta^{m+}} (\mathbf{s}\cdot\mathbf{n}_i)\sin\theta\,\mathrm{d}\theta\,\mathrm{d}\phi \tag{10b}$$

$$\mathbf{s} = \sin\theta\cos\phi\,\mathbf{e}_x + \sin\theta\sin\phi\,\mathbf{e}_y \tag{10c}$$

$$\mathbf{n}_i = \mathbf{n}_{x,i}\,\mathbf{e}_x + \mathbf{n}_{y,i}\,\mathbf{e}_y \tag{10d}$$

$$S_\mathrm{R}^{mn} = (1-\omega_0)I_\mathrm{b} + \frac{\omega_0}{4\pi}\int_{\Omega'=4\pi} I^{m'n'}\mathbf{\Phi}_{m'n'\to mn}\,\mathrm{d}\Omega' \tag{10e}$$

$$\Delta\Omega^m = \int_{\phi^{n-}}^{\phi^{n+}} \int_{\theta^{m-}}^{\theta^{m+}} \sin\theta\,\mathrm{d}\theta\,\mathrm{d}\phi \tag{10f}$$

To relate the intensities on the control-volume surfaces to a nodal one, the step scheme, which is not only simple and convenient, but also ensures positive intensity, is adopted. Then, the final discretized equation for FVM is obtained by

$$a_P^{mn} I_P^{mn} = \sum_{I=E,W,S,N} a_I^{mn} I_I^{mn} + b_P^{mn} \tag{11a}$$

$$a_I^{mn} = -\Delta A_i D_{ci,\mathrm{in}}^{mn} \tag{11b}$$

$$a_P^{mn} = \sum_{I=e,w,s,n} \Delta A_i D_{ci,\mathrm{out}}^{mn} + \beta_{0,P}\Delta V\Delta\Omega^{mn} \tag{11c}$$

$$b_P^{mn} = \left(\beta_0 S_\mathrm{R}^{mn}\right)_P \Delta V \Delta\Omega^{mn} \tag{11d}$$

where

$$D_{ci,\mathrm{out}}^{mn} = \int_{\Delta\Omega^{mn}} (\mathbf{s}\cdot\mathbf{n}_i)\mathrm{d}\Omega\,\mathbf{s}\cdot\mathbf{n}_i > 0 \tag{11e}$$

$$D_{ci,\mathrm{in}}^{mn} = \int_{\Delta\Omega^{mn}} (\mathbf{s}\cdot\mathbf{n}_i)\mathrm{d}\Omega\,\mathbf{s}\cdot\mathbf{n}_i < 0 \tag{11f}$$

A more detailed derivation of the transformations can be found in Refs. [10,22].

4. Results and discussion

4.1. Inverse analysis procedure

In this inverse analysis, the following cases are carried out to verify the performance of RPSO algorithm as an inverse method and to compare its characteristics with HGA and PSO:

(a) Estimation of four wall emissivities ε_w,
(b) Simultaneous estimation of κ_a and σ_s of a gray medium,
(c) Simultaneous estimation of ε_w, κ_a and σ_s.

These parameters are regarded as unknown while the other values such as the temperatures at boundaries, scattering phase function and non-radiative volumetric heat source are assumed to be known. They can be estimated by minimizing objective function, which is expressed by the sum of square errors between estimated and measured temperatures at only four measurement data positions as in

Fig. 2. The objective function for the present inverse radiation analysis is defined by

$$f = \sum_{i=1}^{4} (T_{i,\text{measured}} - T_{i,\text{estimated}})^2 \tag{12}$$

where $T_{i,\text{measured}}$ is the measured temperature from direct problem while $T_{i,\text{estimated}}$ is estimated from inverse analysis with current estimates of the unknown parameters at the measurement location. The number and the position of measured points are selected not only to avoid averaging error effect but also to estimate the parameters effectively as explained in [10].

To minimize objective function, Eq. (12), HGA, PSO and RPSO are adopted and then their estimation results are compared. Because the influence of choosing parameters depends on the combination of their values and actually it is difficult to consider all the values in given ranges one by one, the best performances obtained from each algorithm are presented as representative ones to yield more clear conclusions. The parameters used for each method, such as w, c_i in RPSO, probabilities of crossover and mutation (P_c, P_m) in HGA, are optimized to obtain the best results from several trials by adjusting them in proper ranges (for example, $[0.5, 1.5]$ for w, c_i and $[0.1, 0.9]$ for P_c, P_m). Especially for RPSO and PSO, the recommended ranges of these parameters referred to Clerc's constriction method [23] are as follows:

$$w = \frac{2}{\left|2 - \phi - \sqrt{\phi^2 - 4\phi}\right|}, \quad \text{where } \phi = c_1 + c_2 > 4.0 \tag{13}$$

4.2. Estimation of wall emissivities (cases 1 and 2)

In the first problem, two cases are considered to validate the feasibility of RPSO algorithm for the estimation of four wall emissivities. For case 1, the present estimations obtained by RPSO are compared with the previous results by Kim et al. with HGA [10] to verify if RPSO is an efficient method for inverse radiation analysis. In this case, $\kappa_a = 0.5\ \text{m}^{-1}$ and $\sigma_s = 0.5\ \text{m}^{-1}$, respectively, while the exact values of unknown ε_w's are all set to 0.7.

First of all, the effect of population (swarm) size on computing time with RPSO is compared with HGA and PSO under the same numerical conditions in Ref. [10]. Namely, the computing time is measured for five population sizes such as 10, 50, 100, 150, and 200 after 100 iterations with

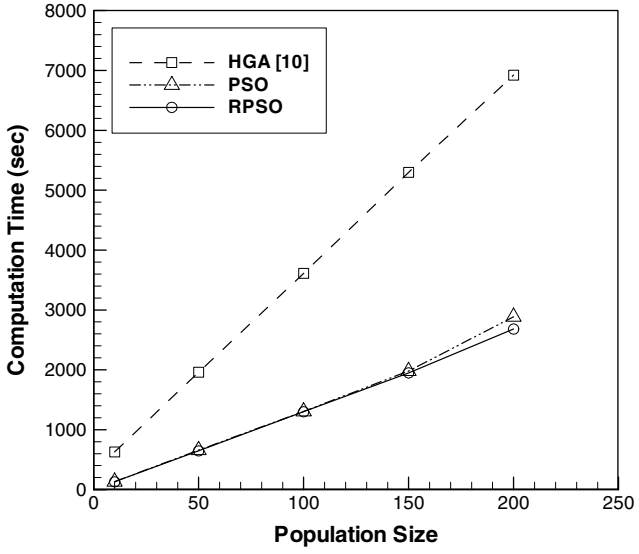

Fig. 4. Comparison of computation time among HGA, PSO and RPSO algorithms (case 1).

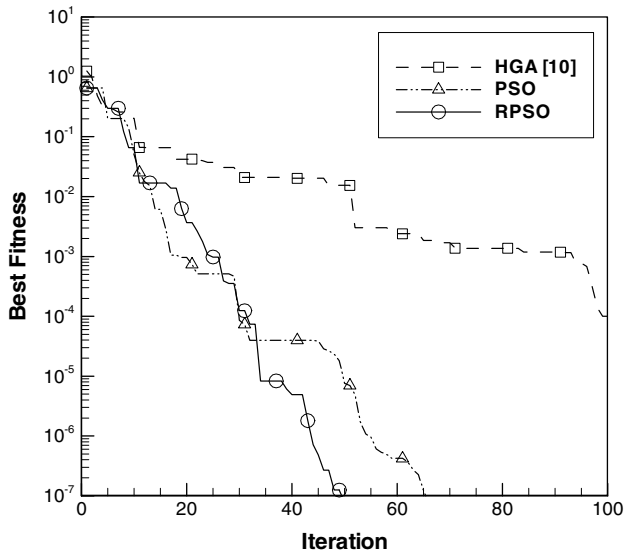

(a) Best fitness

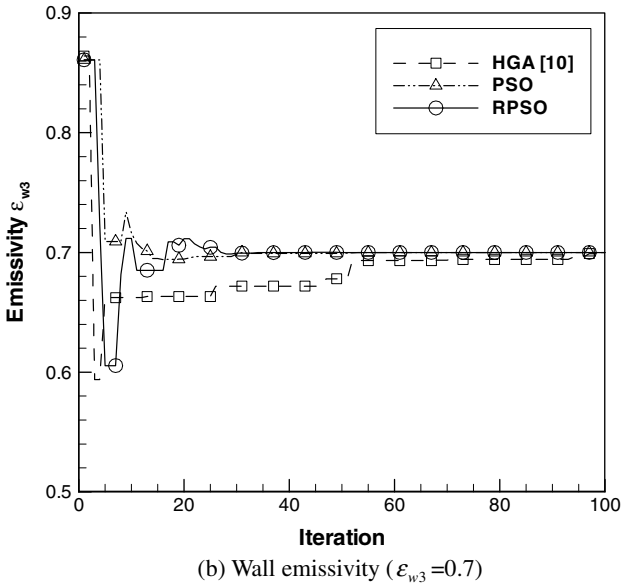

(b) Wall emissivity (ε_{w3} =0.7)

Fig. 5. Comparison of performance among HGA, PSO and RPSO algorithms (case 1).

an Intel P4 2 GHz CPU. As a result, it can be found that the computing time with three algorithms increase directly proportional to population size. However, PSO and RPSO require much shorter time to complete whole iterations than HGA at the same population size in Fig. 4. This is because the search method based on PSO has a much simpler process in finding optimal values rather than the complex operations of GA-based method.

Next, another 100 iterations are conducted to compare the best fitness of objective function, Eq. (12), when RPSO, PSO, and HGA methods are applied with a same population size of 10. Fig. 5(a) shows that the best fitness reach the order of 1×10^{-7} during only about 50 iterations for RPSO and 65 iterations for PSO in a rapid search for a global optimum while HGA converges slowly to the order of 1×10^{-4} even though all 100 iterations are completed. In addition, the estimation process for unknown ε_{w3}, against iteration numbers are investigated to examine performance of each algorithm as shown in Fig. 5(b). While RPSO and PSO are found to converge quickly to 0.7, HGA searches very slowly especially near the exact value without fluctuations even though all three algorithms start with the same initial value 0.86. This fact results from their fundamental principles in the search mechanism. The RPSO as well as PSO has the superior ability of fine local tuning near the optimum value rather than the GA-based method. On the other hand, the whole swarm in PSO and RPSO searches for the better and better solutions following one particle close to a global optimum. Consequently, the best fitness of objective function can converge to the lower order of magnitude rapidly when RPSO and PSO are employed. Similar tendencies are obtained for case 2 with different emissivity values 0.3 instead of 0.7 for top and bottom walls. As shown in Fig. 6, the RPSO and PSO outperform the HGA in searching for exact values of parameters and the convergence speed like case 1.

The final inverse estimations for cases 1 and 2 are summarized in Table 1. The relative errors and their averaged values are presented to compare the accuracy of estimated results and the computing times until the best fitness of objective function reaches less than 1×10^{-6}. For case 1, Intel P4 2 GHz CPU is used, whereas Intel Core 2 Duo 2 GHz CPU is used for case 2 to reduce time. It can be found that all algorithms comparatively estimate ε_w close to real solutions under no measurement error condition. Especially, RPSO calculates the most accurate values within the shortest time when comparing the accuracy of results and the computing time.

4.3. Simultaneous estimation of an absorption and a scattering coefficients (cases 3 and 4)

To verify RPSO in various problems, another two cases are considered for simultaneously estimating κ_a, σ_s of a gray medium. The ε_w's are all known as 0.7, and the exact values of unknown κ_a, σ_s are all 0.5 for case 3, while they are 5.0 and 2.5 for case 4, respectively.

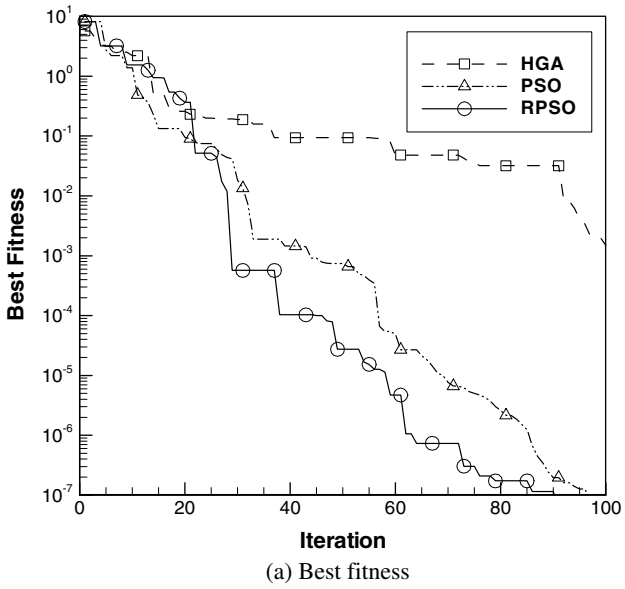

(a) Best fitness

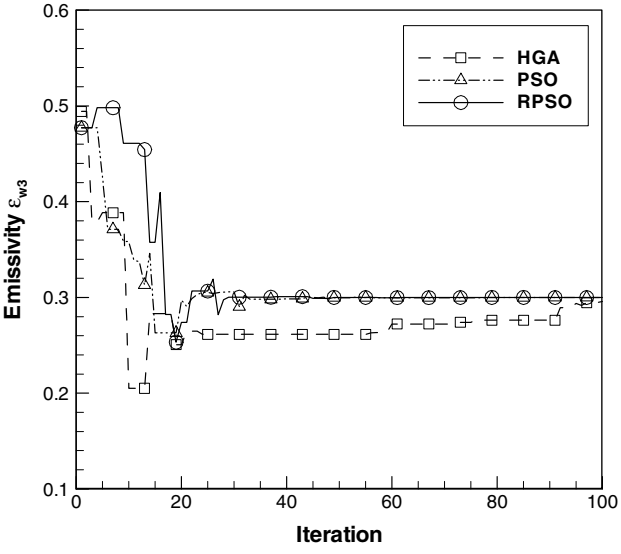

(b) Wall emissivity (ε_{w3} =0.3)

Fig. 6. Comparison of performance among HGA, PSO and RPSO algorithms (case 2).

For both cases, Fig. 7 shows that the best fit results by all three methods rapidly reach less than the order of 1×10^{-6} within the number of 30 iterations. In particular, RPSO and PSO converge further to less than the order of 1×10^{-7} with one more iteration after reaching the order of 1×10^{-6}. For HGA, the convergence speed and the magnitude of the best fitness are greatly improved compared with cases 1 and 2. However, it can be found that the best fitness remains in a premature convergence to 6×10^{-6} order level, which means the individuals do not continue to search for better solutions until 95 iterations as shown in Fig. 7(a). Also, the required iterations for less than the order of 1×10^{-6} in HGA are not uniform depending on the unknown parameters such that 14 iterations for $\kappa_a = 0.5\ m^{-1}$, $\sigma_s = 0.5\ m^{-1}$ and 25 iterations for

Table 1
Comparison of estimation results for inverse wall emissivity

Parameter	Case 1 ($\varepsilon_{w1,2,3,4} = 0.7$)			Case 2 ($\varepsilon_{w1,2} = 0.7$, $\varepsilon_{w3,4} = 0.3$)		
	HGA[a] [10]	PSO	RPSO	HGA[a]	PSO	RPSO
ε_{w1}	0.6969	0.7000	0.6999	0.7047	0.7001	0.7001
(Rel. error %)	(0.44)	(0.0)	(0.01)	(0.67)	(0.01)	(0.01)
ε_{w2}	0.7006	0.7001	0.7000	0.7001	0.7001	0.7001
(Rel. error %)	(0.09)	(0.01)	(0.0)	(0.01)	(0.01)	(0.01)
ε_{w3}	0.7000	0.6999	0.7000	0.2959	0.2999	0.2999
(Rel. error %)	(0.0)	(0.01)	(0.0)	(1.37)	(0.03)	(0.03)
ε_{w4}	0.7027	0.7002	0.7001	0.3039	0.2999	0.3000
(Rel. error %)	(0.39)	(0.03)	(0.01)	(1.30)	(0.03)	(0.0)
Averaged Rel. error (%)	0.23	0.01	0.005	0.84	0.02	0.01
Computational time (s)	629.2	127.9	71.3	191.6	94.4	71.7

[a] Measured after 100 iterations.

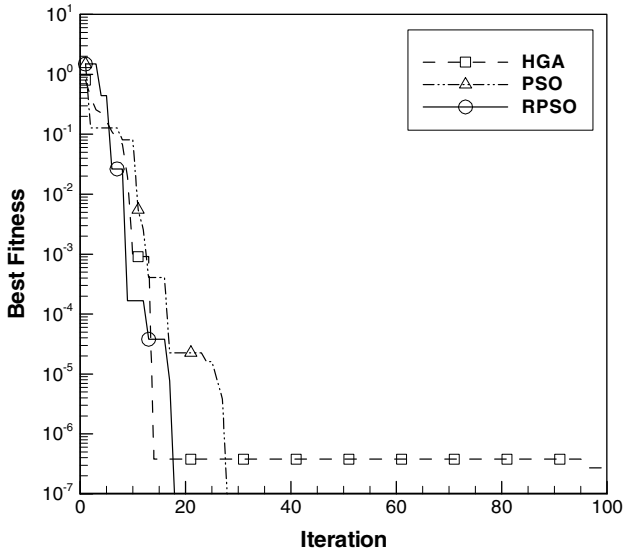

(a) Case 3 (κ_a =0.5 m^{-1}, σ_s = 0.5 m^{-1})

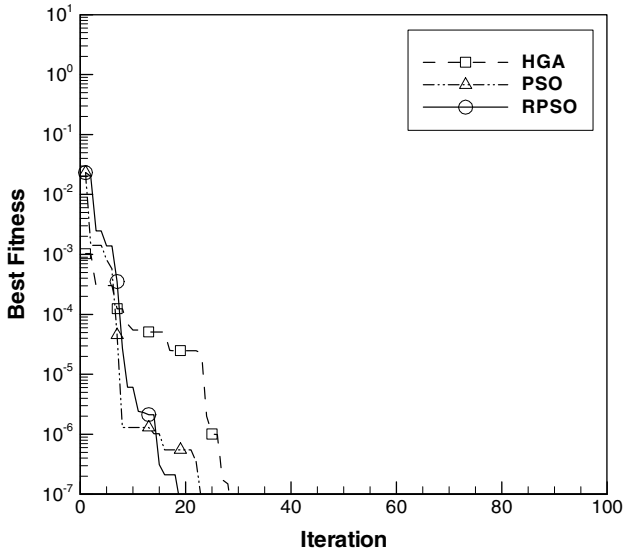

(b) Case 4 (κ_a =5.0 m^{-1}, σ_s = 2.5 m^{-1})

Fig. 7. Comparison of best fitness among HGA, PSO and RPSO algorithms (cases 3 and 4).

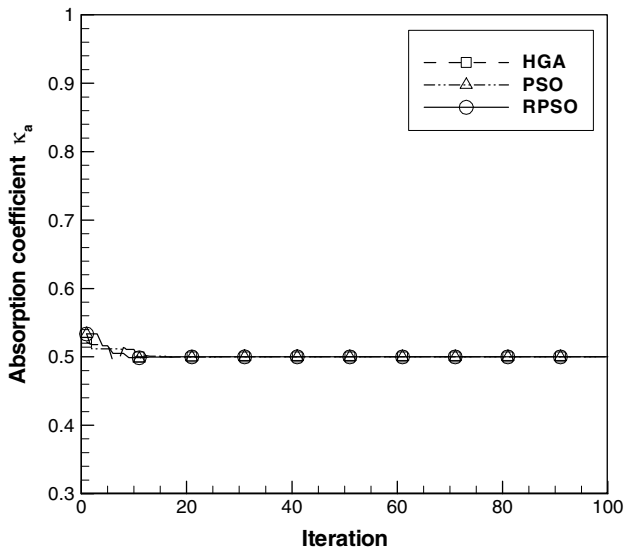

(a) Case 3 (κ_a =0.5 m^{-1})

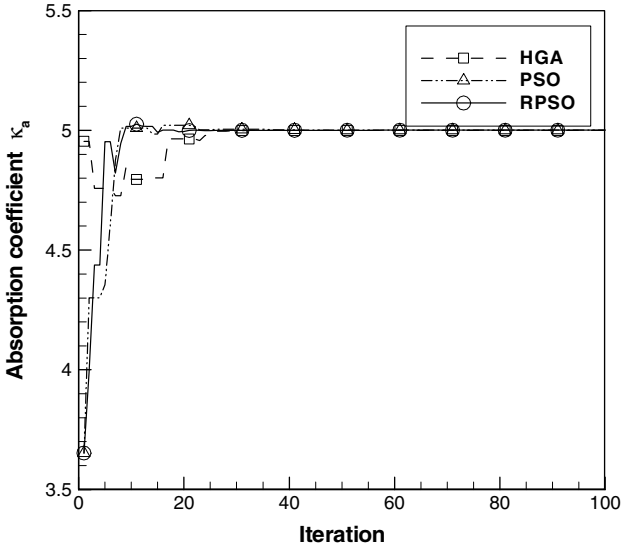

(b) Case 4 (κ_a =5.0 m^{-1})

Fig. 8. Comparison of absorption coefficient estimations (cases 3 and 4).

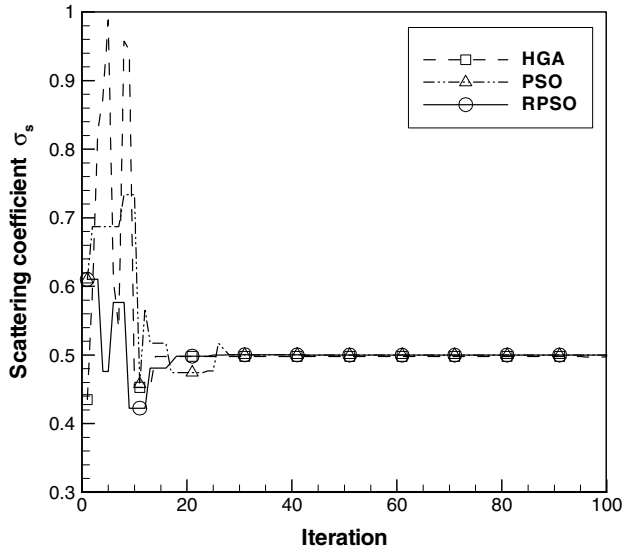

(a) Case 3 ($\sigma_s = 0.5\ \mathrm{m}^{-1}$)

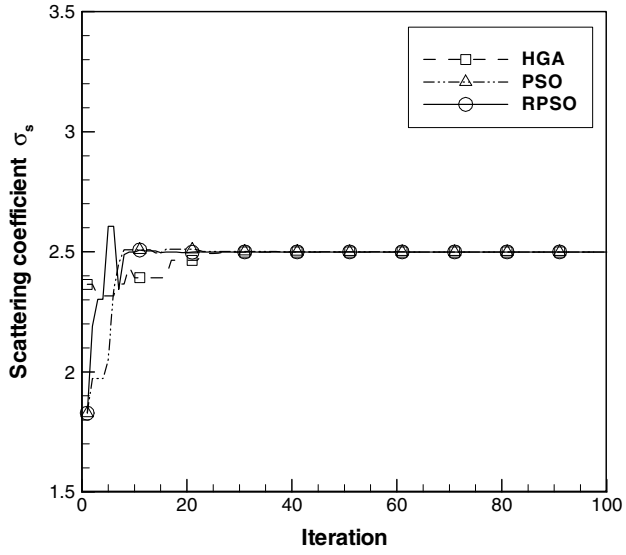

(b) Case 4 ($\sigma_s = 2.5\ \mathrm{m}^{-1}$)

Fig. 9. Comparison of scattering coefficient estimations (cases 3 and 4).

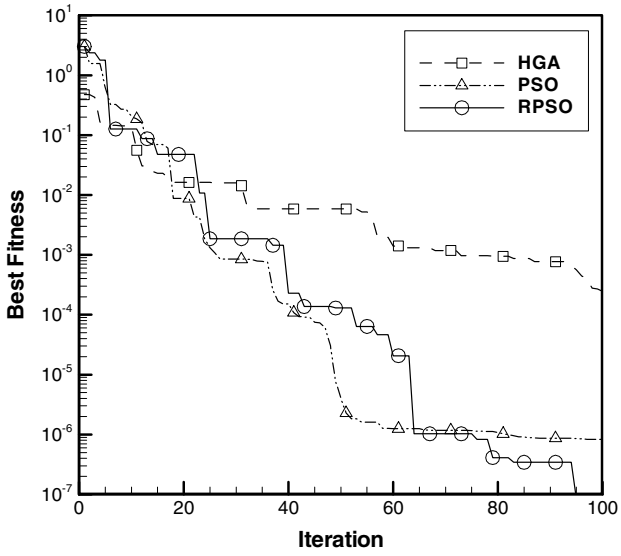

(a) Best fitness

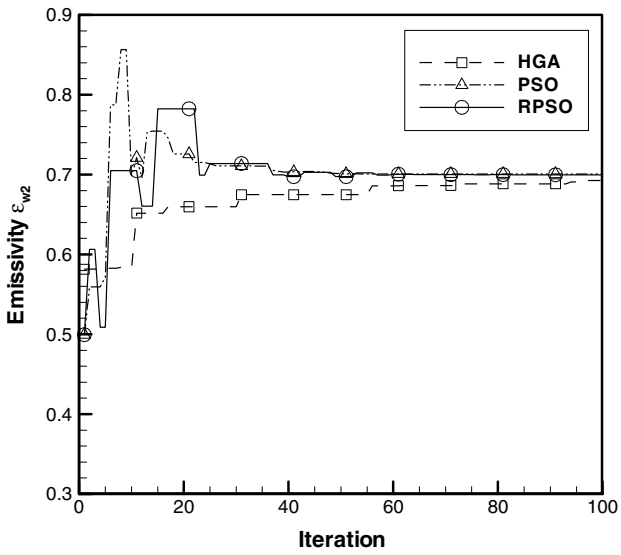

(b) Wall emissivity (ε_{w2}=0.7)

Fig. 10. Comparison of performance among HGA, PSO and RPSO algorithms (case 5).

$\kappa_a = 5.0\ \mathrm{m}^{-1}$, $\sigma_s = 2.5\ \mathrm{m}^{-1}$. Variation of each κ_a and σ_s against iteration is presented in Fig. 8 for case 3 and in Fig. 9 for case 4. It can be clearly seen that both RPSO and PSO search faster than HGA, even though they start with initial values located far from the solutions. Consequently, it can be concluded that the search capability for global optimum as well as the fine local tuning near the

Table 2
Comparison of estimation results for inverse absorption and scattering coefficients

Parameter	Case 3 ($\kappa_a = 0.5$, $\sigma_s = 0.5$)			Case 4 ($\kappa_a = 5.0$, $\sigma_s = 2.5$)		
	HGA	PSO	RPSO	HGA	PSO	RPSO
κ_a	0.5000	0.5000	0.5000	4.9968	5.0215	4.9918
(Rel. error %)	(0.0)	(0.0)	(0.0)	(0.06)	(0.43)	(0.16)
σ_s	0.4980	0.5003	0.4984	2.4942	2.5102	2.4967
(Rel. error %)	(0.40)	(0.06)	(0.32)	(0.23)	(0.41)	(0.13)
Averaged Rel. error (%)	0.20	0.03	0.16	0.15	0.42	0.15
Computational time (s)	17.3	22.3	13.9	143.4	58.8	55.1

solutions of RPSO and PSO are comparatively better than those of HGA.

On the other hand, Park and Yoon [24] introduced a two-stage estimation process by the CGM to estimate κ_a and σ_s at the same time in 3D participating media radiation–conduction. Because these parameters are strongly coupled in the sensitivity equations and there is a great difference between the sensitivity values of temperature with respect to each parameter, the simultaneous estimation of these parameters is very difficult unless the initial values are chosen near the exact values. Therefore, they obtain converged estimation of κ_a with assumed σ_s at first stage, and then estimate those two parameters simultaneously. While this method has some drawbacks such that a preposterous value can be obtained depending on the assumption of initial values and the estimation process is too complicated, the PSO-based methods in the present study is able to easily find solutions without such difficulty.

The final estimations for cases 3 and 4 with three algorithms until the best fitness of objective function reaches less than 1×10^{-6} using Intel Core 2 Duo 2 GHz CPU are summarized in Table 2. It reveals for both cases that RPSO consistently estimates the relatively accurate optimum values within the shortest time among other methods even with poor initial values.

4.4. Simultaneous estimation of emissivities, absorption and scattering coefficients (cases 5 and 6)

Finally, a simultaneous estimation of ε_w, κ_a and σ_s is considered to verify the performance of RPSO in the multi-parameter inverse problem. While two emissivities of side walls ε_{w1}, ε_{w2} are unknown for case 5, all four ε_w are to be predicted for case 6. The exact values of all ε_w's are 0.7 and those of unknown κ_a and σ_s are 0.5 m^{-1} for both cases.

It can be seen from Fig. 10(a) that the best fitness of PSO converges slowly after 50 iterations even though it reaches very close to the order of 1×10^{-6} quickly among other methods. The main reason exists in the drawback of PSO such that even if it falls into a premature convergence, thereafter it remains in the local optimum as explained above while RPSO continues to converge to less than the order of 1×10^{-7} searching for better solutions. This leads to yielding a great improvement in accuracy of estimation results by RPSO as listed in Table 3. As shown in Fig. 10(b), the predictions by RPSO and PSO converge more quickly to the exact value 0.7 of ε_{w2} than by HGA.

For case 6 with a total of six unknown parameters with ε_w, κ_a and σ_s, it is found that all algorithms fail in estimating exact solutions due to a lack of physical information with four temperature measurements. Therefore, the measurement points are increased to nine, whereas a number of iterations are extended from 100 to 3000. Thereby, inverse solutions can be obtained from all three methods as shown in Fig. 11 and in Table 3. Similar to previous cases, the results show an excellent performance by RPSO compared with the other methods in convergence rate as well as estimation accuracy. On the other hand, HGA is observed not to outperform PSO-based methods for both cases, and shows a very slow convergence when the number of unknown parameters is increased. The result clearly shows that the performance of HGA is the highest with two unknown ε_w's, but it exhibits a distinguished drop in efficiency as the number of unknown ε_w is higher than two. A similar result was also observed by Verma and Balaji [25] who found that GA is not very efficient for simultaneous estimation of more than two parameters unless there is a fair idea of ranges in which the parameters may lie when applied to a combined conduction–radiation problem from 1D plane parallel with participating medium.

Table 3
Comparison of estimation results for inverse wall emissivity, absorption and scattering coefficients

Parameter	Case 5 ($\varepsilon_{w1,2} = 0.7$, $\kappa_a = 0.5$, $\sigma_s = 0.5$)			Case 6 ($\varepsilon_{w1,2,3,4} = 0.7$, $\kappa_a = 0.5$, $\sigma_s = 0.5$)		
	HGA[a]	PSO	RPSO	HGA[b]	PSO	RPSO
ε_{w1}	0.6913	0.7013	0.6997	0.7012	0.7007	0.6993
(Rel. error %)	(1.24)	(0.19)	(0.04)	(0.17)	(0.10)	(0.10)
ε_{w2}	0.6952	0.7008	0.6999	0.7006	0.7006	0.6994
(Rel. error %)	(0.69)	(0.11)	(0.01)	(0.09)	(0.09)	(0.09)
ε_{w3}	–	–	–	0.7037	0.7006	0.6994
(Rel. error %)				(0.53)	(0.09)	(0.09)
ε_{w4}	–	–	–	0.7032	0.7005	0.6996
(Rel. error %)				(0.46)	(0.07)	(0.06)
κ_a	0.5025	0.4995	0.5001	0.4988	0.4997	0.5003
(Rel. error %)	(0.50)	(0.10)	(0.02)	(0.24)	(0.06)	(0.06)
σ_s	0.5393	0.4851	0.4997	0.5058	0.5011	0.4989
(Rel. error %)	(7.86)	(2.98)	(0.06)	(1.16)	(0.22)	(0.22)
Averaged Rel. error (%)	2.57	0.32	0.08	0.44	0.11	0.10
Computational time (s)	141.3	61.6	59.6	5053.1	2205.6	2087.4

[a] Measured after 100 iterations.
[b] Measured after 3000 iterations.

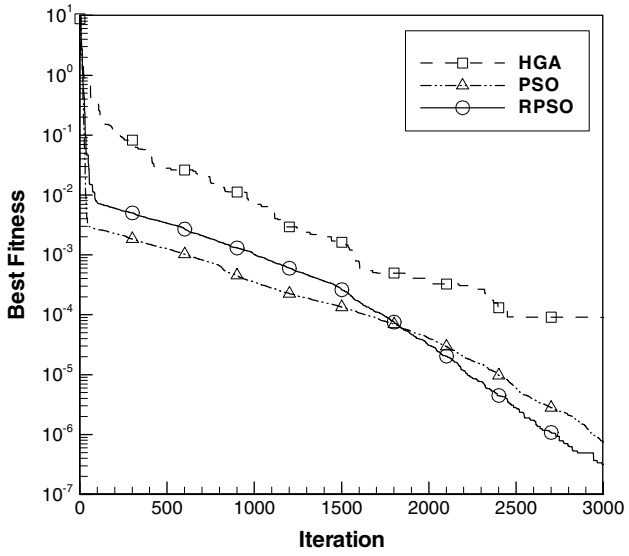

(a) Best fitness

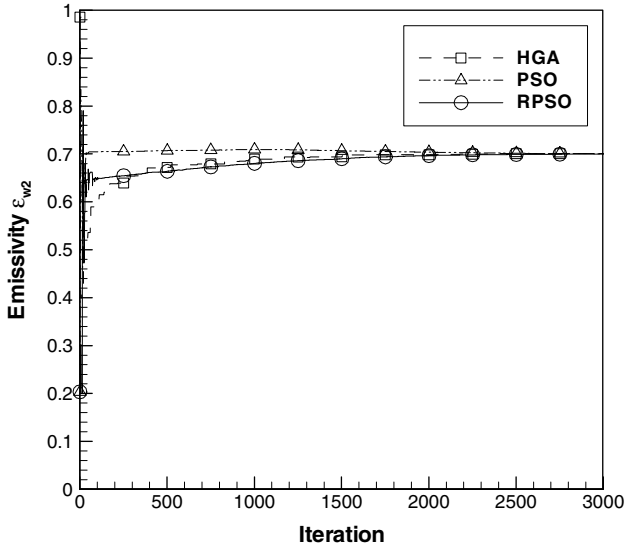

(b) Wall emissivity (ε_{w2}=0.7)

Fig. 11. Comparison of performance among HGA, PSO and RPSO algorithms (case 6).

To examine the effect of measurement errors on accuracy of the estimation using RPSO, measurement errors are simulated by adding an error term as follows [10]:

$$(T_i)_{\text{measured}} = (T_i)_{\text{exact}} + \sigma_{\text{st}}\zeta, \quad i = 1\text{–}9 \tag{14}$$

where ζ is a normal distributed random variable with zero mean and unit standard deviation. σ_{st}, which is a standard deviation of measured temperatures for a measured error γ at 99% confidence, is determined by

$$\sigma_{\text{st}} = \frac{T_{\text{exact}} \times \gamma}{2.576} \tag{15}$$

Table 4 shows the accuracy of estimations with various standard deviations for three cases. It shows that increasing σ_{st} decreases the accuracy of the estimations. But it is observed that the satisfied estimation of unknown parameters can be obtained by RPSO algorithm.

5. Conclusions

The inverse radiation analysis is carried out for estimating the radiative parameters for an absorbing, emitting and scattering media in a 2D irregular geometry with diffusely emitting and reflecting opaque boundaries from the temperature measurements. The FVM is employed to solve the radiative transfer equation of the direct problem. In order to verify the feasibility and the performance of the RPSO, which is one of global search-based methods, combined problems of unknown ε_{w}, κ_{a} and σ_{s} are inversely estimated. A total of six cases are investigated depending on the combination of unknown parameters to compare the overall characteristics of RPSO with PSO and HGA. The best results obtained from each algorithm are presented as representative ones to yield more clear conclusions because values obtained are not different much depending on the selection of parameters in given ranges. Based on the results, it is sufficiently observed that the RPSO has better computational performance than the other two algorithms. Moreover, it shows a robust performance even for

Table 4
Comparison of measurement errors using RPSO for different standard deviations

Parameter	Case 1 ($\varepsilon_{w1,2,3,4} = 0.7$)		Case 3 ($\kappa_a = 0.5$, $\sigma_s = 0.5$)		Case 6 ($\varepsilon_{w1,2,3,4} = 0.7$, $\kappa_a = 0.5$, $\sigma_s = 0.5$)	
	$\sigma_{st} = 0.05$	$\sigma_{st} = 0.1$	$\sigma_{st} = 0.05$	$\sigma_{st} = 0.1$	$\sigma_{st} = 0.05$	$\sigma_{st} = 0.1$
ε_{w1}	0.6863	0.6726	–	–	0.6981	0.6990
(Rel. error %)	(1.96)	(3.91)			(0.27)	(0.14)
ε_{w2}	0.6955	0.6909	–	–	0.7035	0.7097
(Rel. error %)	(0.64)	(1.30)			(0.50)	(1.39)
ε_{w3}	0.6970	0.6940	–	–	0.7012	0.7047
(Rel. error %)	(0.43)	(0.86)			(0.17)	(0.67)
ε_{w4}	0.7179	0.7359	–	–	0.7263	0.7554
(Rel. error %)	(2.56)	(5.13)			(3.76)	(7.91)
κ_a	–	–	0.4992	0.4984	0.4963	0.4915
(Rel. error %)			(0.16)	(0.32)	(0.74)	(1.70)
σ_s	–	–	0.4711	0.4422	0.4878	0.4803
(Rel. error %)			(5.78)	(11.56)	(2.44)	(3.94)
Averaged Rel. error (%)	1.40	2.80	2.97	5.94	1.31	2.63

simultaneous estimation of strongly-coupled multi-parameter environment. Finally, the effects of measurement errors on the accuracy of estimation are carefully examined. Consequently, it can be concluded that the RPSO has been successfully verified as an effective method for the inverse radiation analysis.

Acknowledgement

This work was supported by Grant No. R01-2006-000-11311-0 from the Basic Research Program of the Korea Science and Engineering Foundation.

References

[1] M.N. Özisik, H.R.B. Orlande, Inverse Heat Transfer, Taylor & Francis, New York, 2000.
[2] L.H. Liu, H.P. Tan, Q.Z. Yu, Simultaneous identification of temperature profile and wall emissivities in semitransparent medium by inverse radiation analysis, Numer. Heat Transfer, Part A 36 (1999) 511–525.
[3] Y.K. Hong, S.W. Baek, Inverse radiation problem in determination of the inlet temperature profile for two-phase laminar flow in a channel, Numer. Heat Transfer, Part A 50 (2006) 1–19.
[4] N.R. Ou, C.H. Wu, Simultaneous estimation of extinction coefficient distribution, scattering albedo and phase function of a two-dimensional medium, Int. J. Heat Mass Transfer 45 (2002) 4663–4674.
[5] C.H. Huang, M.N. Özisik, Inverse problem of determining unknown wall heat in laminar flow through a parallel plate, Numer. Heat Transfer, Part A 21 (1992) 55–70.
[6] J.C. Bokar, M.N. Özisik, Inverse analysis for estimating the time varying inlet temperature in laminar flow inside a parallel plate duct, Int. J. Heat Mass Transfer 38 (1995) 39–45.
[7] Y.K. Hong, S.W. Baek, Inverse analysis for estimating the unsteady inlet temperature distribution for two-phase laminar flow in a channel, Int. J. Heat Mass Transfer 49 (2006) 1137–1147.
[8] K.W. Kim, S.W. Baek, H.S. Ryu, Comparison of optimization techniques for an inverse radiation boundary problem, Int. Conf. Comput. Methods (2004) 15–17.
[9] H.Y. Li, C.Y. Yang, A genetic algorithm for inverse radiation problems, Int. J. Heat Mass Transfer 40 (1997) 1545–1549.
[10] K.W. Kim, S.W. Baek, M.Y. Kim, H.S. Ryu, Estimation of emissivities in a two-dimensional irregular geometry by inverse radiation analysis using hybrid genetic algorithm, J. Quant. Spectrosc. Radiat. 87 (2004) 1–14.
[11] J.C. Becceneri, S. Stephany, H.F. de Campos Velho, A.J. Silva Neto, Solution of the inverse problem of radiative properties estimation with particle swarm optimization techniques, Inverse Probl. Eng. Seminar (IPES) (2006).
[12] Z. Michalewicz, Genetic Algorithms + Data Structures = Evolution Programs, Springer, New York, 1999.
[13] S. Joachim, Parallel Genetic Algorithms: Theory and Applications, IOS Press, Amsterdam, 1993.
[14] K.F. Man, K.S. Tang, S. Kwong, Genetic Algorithms: Concepts and Designs, Springer, London, 1999.
[15] J. Kennedy, R. Eberhart, Particle swarm optimization, in: Proceedings of the IEEE International Conference on Neural Networks, 1995, pp. 1942–1945.
[16] R.C. Eberhart, P. Simpson, R. Dobbins, Computational Intelligence PC Tools, Academic Press, Boston, 1996.
[17] M. Clerc, Particle Swarm Optimization, ISTE Ltd., London, 2006.
[18] E. Ozcan, C. Mohan, Particle swarm optimization: surfing the waves, in: Proceedings of the Congress on Evolutionary Computation, 1999, pp. 1939–1944.
[19] K. James, C.E. Russell, S. Yuhui, Swarm Intelligence, Morgan Kaufman, San Francisco, 2001.
[20] O. Urfalioglu, Robust estimation of camera rotation, translation and focal length at high outlier rates, Comput. Robot Vis. Proc. (2004) 464–471.
[21] J. Liu, H.M. Shang, Y.S. Chen, T.S. Wang, Prediction of radiative transfer in general body-fitted coordinates, Numer. Heat Transfer, Part B 31 (1997) 423–439.
[22] S.W. Baek, M.Y. Kim, J.S. Kim, Nonorthogonal finite-volume solutions of radiative heat transfer in a three-dimensional enclosure, Numer. Heat Transfer, Part B 34 (1998) 419–437.
[23] M. Clerc, J. Kennedy, The particle swarm-explosion, stability, and convergence in a multidimensional complex space, IEEE Trans. Evol. Comput. 6 (2002) 58–73.
[24] H.M. Park, T.Y. Yoon, Solution of the inverse radiation problem using a conjugate gradient method, Int. J. Heat Mass Transfer 43 (2000) 1767–1776.
[25] S. Verma, C. Balaji, Multi-parameter estimation in combined conduction–radiation from a plane parallel participating medium using genetic algorithms, Int. J. Heat Mass Transfer 50 (2007) 1706–1714.